

Interatomic potentials for atomistic simulations of the Ti-Al system

Rajendra R. Zope and Y. Mishin*

School of Computational Sciences, George Mason University, Fairfax, VA 22030

(Dated: October 26, 2018)

Abstract

Semi-empirical interatomic potentials have been developed for Al, α -Ti, and γ -TiAl within the embedded atom method (EAM) formalism by fitting to a large database of experimental as well as *ab-initio* data. The *ab initio* calculations were performed by the linearized augmented plane wave (LAPW) method within the density functional theory to obtain the equations of state for a number of crystal structures of the Ti-Al system. Some of the calculated LAPW energies were used for fitting the potentials while others for examining their quality. The potentials correctly predict the equilibrium crystal structures of the phases and accurately reproduce their basic lattice properties. The potentials are applied to calculate the energies of point defects, surfaces, and planar faults in the equilibrium structures. Unlike earlier EAM potentials for the Ti-Al system, the proposed potentials provide a reasonable description of the lattice thermal expansion, demonstrating their usefulness for molecular dynamics and Monte Carlo simulations at high temperatures. The energy along the tetragonal deformation path (Bain transformation) in γ -TiAl calculated with the EAM potential is in a fairly good agreement with LAPW calculations. Equilibrium point defect concentrations in γ -TiAl are studied using the EAM potential. It is found that antisite defects strongly dominate over vacancies at all compositions around stoichiometry, indicating that γ -TiAl is an antisite disorder compound in agreement with experimental data.

PACS numbers: 61.72,62.20.Dc,64.30.+t,65.40

Keywords: EAM, vacancy, stacking fault, point defect, thermal expansion, elastic constants, TiAl

I. INTRODUCTION

In the recent years, intermetallics alloys based on the gamma titanium aluminide TiAl have been the subject of intense research due to their potential for applications in the aerospace and automobile industries.^{1,2,3,4} Such alloys have an excellent oxidation and corrosion resistance which, combined with good strength retention ability and low density, make them very advanced high temperature materials. A study of fundamental properties such as the nature of interatomic bonding, stability of crystal structures, elastic properties, dislocations, grain boundaries, interfaces, as well as point defects and diffusion are therefore warranted in order to gain more insight into the behavior of these intermetallic alloys under high temperatures and mechanical loads. Over the past few years, numerous investigations, both experimental and theoretical, have been devoted to the study of such properties.^{5,6,7,8,9,10,11,12,13} Accurate *ab-initio* studies of the structural stability, elastic properties, and the nature of interatomic bonding have been reported for γ -TiAl as well as other stoichiometric alloys of the Ti-Al system.^{14,15,16} However, the application of *ab-initio* methods to atomistic studies of diffusion, deformation, and fracture are limited due to the prohibitively large computational resources required for modeling point defects, dislocations, grain boundaries, and fracture cracks. Such simulations require large simulation cells and computationally demanding techniques such as molecular dynamics and Monte Carlo. Semiempirical methods employing model potentials constructed by the embedded atom method (EAM)^{17,18,19} or the equivalent Finnis-Sinclair (FS) method²⁰ are particularly suitable for this purpose. These methods provide a way of modeling atomic interactions in metallic systems in an approximate manner allowing fast simulations of large systems. Several studies applying these methods to a variety of properties of γ -TiAl such as planar faults, dislocations, and point defects have been reported in the literature.^{12,21,22} The effectiveness of semiempirical methods obviously depends upon the quality of the model potentials employed. Recent studies^{23,24,25,26,27,28,29,30,31,32} have shown that the incorporation of *ab-initio* data during the fitting of interatomic potentials can significantly enhance their ability to mimic interatomic interactions. For example, Bakes *et al.*³² examined the range of interatomic forces in aluminum using model potentials and *ab-initio* methods. They found that potentials that included *ab-initio* data during the fitting procedure could reproduce

ab-initio forces much more accurately than potentials fit to experimental data only.

In the present work we explore the possibility of constructing a reliable interatomic potential for the Ti-Al system. To this end, we develop EAM-type interatomic potentials for γ -TiAl and the component elements Ti and Al by fitting to a large database of experimental properties and *ab-initio* structural energies of these phases. The *ab-initio* database has been generated by density functional calculations using the linearized augmented plane wave (LAPW) method within the generalized gradient approximation (GGA) for the exchange-correlation effects. The *ab-initio* data are used in the form of energy-volume relations (equations of state) of various structures of Al, Ti, and γ -TiAl. The energy along the Bain transformation path between the L1₀ and B2 structures of TiAl has also been calculated in this work.

While many EAM-type potentials have been reported for Al,^{23,28,32,33,34} relatively few attempts have been made to create such potentials for Ti^{35,36,37} and TiAl.^{21,22,38,39,40,41,42} Titanium, like other transition metals, cannot be expected to follow the EAM model as accurately as noble metals usually do. In contrast, Al is known to lend itself to the EAM description quite readily.^{23,28,32,33,34} The γ -TiAl compound is probably a borderline case. Some of the previous EAM potentials for γ -TiAl had a reasonable success in modeling lattice properties and extended lattice defects.^{21,22,38} On the other hand, Paidar *et al.*⁴³ calculated deformation paths between different structures of TiAl by an *ab-initio* method and with a Finnis-Sinclair potential and found only a qualitative agreement between the two calculation methods. In this work we are trying to gain a better understanding of the applicability range of the EAM model for γ -TiAl. In particular, we want explore the possibility of obtaining a high-quality EAM potential for γ -TiAl by incorporating *ab-initio* data into the fitting database. Our results suggest that the quality of an EAM potential can indeed be improved this way, and that the potential proposed here can be useful for atomistic simulations of γ -TiAl.

II. CONSTRUCTION OF EAM POTENTIALS

A. Database of fitted physical properties

We have first constructed EAM potentials for pure Al and Ti followed by fitting a cross-interaction potential Ti-Al. The database of physical properties employed in the fitting procedure consisted of two categories. The first category is comprised of experimental data for the lattice constant, c/a ratio, cohesive energy, and elastic constants. For pure Al and Ti it also included the vacancy formation energy and the linear thermal expansion factors at several temperatures. The second set of properties consisted of *ab-initio* energy differences between various crystal structures. Such differences are necessary to ensure the correct stability of the experimentally observed ground state structures against other possible structures and to sample a large area of configuration space away from equilibrium.

The *ab-initio* database consists of energy versus volume (EV) relations for various crystal structures. For Al, EV curves were computed here for the face centered cubic (fcc), hexagonal closed packed (hcp), body centered cubic (bcc), simple cubic (sc), diamond, and the $\text{I}10$ structures. The $\text{I}10$ structure of Al is a defected fcc lattice with a vacancy in the corner of each cubic unit cell. In the case of titanium, EV curves were generated in Ref. 44 for the hcp, fcc, bcc, sc, and the omega (C32) structures. For the intermetallic compound TiAl, EV relations were obtained in this work for three structures: $\text{I}10$ (CuAu prototype), B2 (CsCl prototype), and B1 (NaCl prototype). Each EV curve typically consists of total energies for about 20-30 different volumes around the equilibrium volume. The c/a ratio of the $\text{I}10$ structure has been optimized at each volume. As the *ab-initio* and EAM energies are at different scales, all *ab-initio* energies for a given element or compound of a given stoichiometry were shifted so that to match the experimental cohesive energy of the equilibrium ground state structure. This procedure is followed merely to facilitate the comparison of structural energies calculated by different methods and does not introduce any new approximation. The equilibrium energy of the $\text{D}0_{19}\text{-Ti}_3\text{Al}$ compound has also been calculated here to check the methodology and provide useful reference information. The energy of this phase was minimized with respect to its volume while keeping the c/a ratio fixed at the value found in Ref. 45.

The EV curves were calculated using the full potential LAPW method^{46,47,48} within the

Hohenberg-Kohn-Sham formulation of the density functional theory.^{49,50,51} The calculations were carried out in a spin-restricted mode and the exchange-correlation effects were treated at the level of the GGA. The *EV* calculations for Ti were carried out using an LAPW code available at the Naval Research Laboratory and were reported in Ref. 44. The calculations for Al, TiAl and Ti₃Al were performed in this work and employed the WIEN2K package.⁵² The Perdew-Wang^{53,54,55} (PW91) exchange-correlation functional was used for Ti calculations,⁴⁴ while its simplified and more efficient version referred to in literature as PBE⁵⁶ was used for Al and TiAl. The muffin-tin radii of Al and Ti were chosen to be 2 a.u. For each crystal structure, systematic \mathbf{k} point and basis set convergence tests were carried out at a fixed volume near equilibrium volume. The same set of parameters was subsequently employed for different volumes as well as for the Bain path calculations. The accuracy of the LAPW total energies calculated in the present work was estimated to be better than 0.5 mRy/atom.

We now describe some relevant details of the potential fitting procedure. In the embedded atom formalism,^{17,18} the total energy of a system is expressed as

$$E_{tot} = \frac{1}{2} \sum_{i,j} \Phi_{ij}(r_{ij}) + \sum_i F_i(\bar{\rho}_i). \quad (1)$$

Here, Φ_{ij} is the pair-interaction energy between atom i and j at positions \vec{r}_i and \vec{r}_j , and F_i is the embedding energy of atom i . The $\bar{\rho}_i$ in Eq. (1) is the host electron density at site i induced by all other atoms in the system. The latter is given by

$$\bar{\rho}_i = \sum_{j \neq i} \rho_j(r_{ij}). \quad (2)$$

For a binary system A-B, the total energy given by Eq. (1) is invariant with respect to the

following set of transformations:^{31,57}

$$\rho_A(r) \rightarrow s_A \rho_A(r), \quad (3)$$

$$\rho_B(r) \rightarrow s_B \rho_B(r), \quad (4)$$

$$F_A(\bar{\rho}) \rightarrow F_A(\rho_A(r)/s_A), \quad (5)$$

$$F_B(\bar{\rho}) \rightarrow F_B(\rho_B(r)/s_B), \quad (6)$$

$$F_A(\bar{\rho}) \rightarrow F_A(\bar{\rho}) + g_A \bar{\rho}, \quad (7)$$

$$F_B(\bar{\rho}) \rightarrow F_B(\bar{\rho}) + g_B \bar{\rho}, \quad (8)$$

$$\Phi_{AA}(r) \rightarrow \Phi_{AA}(r) - 2g_A \rho_A(r), \quad (9)$$

$$\Phi_{BB}(r) \rightarrow \Phi_{BB}(r) - 2g_B \rho_B(r), \quad (10)$$

$$\Phi_{AB}(r) \rightarrow \Phi_{AB}(r) - 2g_A \rho_A(r) - 2g_B \rho_B(r), \quad (11)$$

where A and B refer to the type of element (Al or Ti) and s_A, s_B, g_A , and g_B are arbitrary constants. For any particular compound, the potential can be cast into the so-called effective pair format⁵⁷ by choosing $g_A = -F'_A(\bar{\rho}_A^0)$ and $g_B = -F'_B(\bar{\rho}_B^0)$, where $\bar{\rho}_A^0$ and $\bar{\rho}_B^0$ are the equilibrium electron densities on atoms in the compound. The effective pair format provides a convenient way of comparing different potentials for the same compound.

An EAM potential for a binary system can be constructed by two different procedures. One is to optimize all potential functions simultaneously during a single fit, as it was done for example for the Ni-Al system.³¹ This scheme offers the advantage of having many parameters available for fitting to properties of a selected alloy or compound. However, it suffers from the drawback that the quality of potentials for pure elements (Al and Ti in our case) is often poor. An alternative and more common approach is to separately develop accurate EAM potentials for pure elements and use them to fit the cross potential for alloys (compounds). We resort to the latter procedure for the Ti-Al system. The parametrization of potential functions employed in the fitting procedure is discussed below.

B. EAM potential for Al

For the EAM potential for Al, we chose the electron density function in the form

$$\rho(r) = \psi \left(\frac{r - r_c}{h} \right) \left\{ A_0 (r - r_0)^y e^{-\gamma(r - r_0)} \right. \\ \left. \times \left(1 + B_0 e^{-\gamma(r - r_0)} \right) + C_0 \right\}, \quad (12)$$

Here, $A_0, B_0, C_0, r_0, r_c, h, y$ and γ are the fitting parameters and $\psi(x)$ is a cutoff function defined as

$$\begin{aligned}\psi(x) &= 0 \quad \text{for } x \geq 0 \\ &= \frac{x^4}{(1+x^4)} \quad \text{for } x < 0,\end{aligned}\quad (13)$$

where r_c is the cutoff distance. The electron density in equilibrium fcc Al is normalized to unity, i.e. $\bar{\rho} = \sum_j N_j \rho_j = 1$, where j runs over coordination shells and N_j is the number of atoms on the j -th coordination shell. This constraint fixes one parameter in the above set of parameters. The pair interaction function is parametrized in the form

$$\Phi(r) = \left[\frac{V_0}{(b_2 - b_1)} \left(\frac{b_2}{z^{b_1}} - \frac{b_1}{z^{b_2}} \right) + \delta \right] \psi\left(\frac{r - r_c}{h}\right), \quad (14)$$

where, $z = r/r'$, and b_1, b_2, δ, V_0 , and r' are fitting parameters. Thus, altogether we have 12 fitting parameters for functions $\rho(r)$ and $\Phi(r)$.

The embedding energy is obtained by equating the energy of fcc Al [Eq. (1)] to the universal equation of state (EOS). By studying a broad range of materials, Rose *et al.*⁵⁸ proposed the “universal” EOS in the form

$$E(r) = -E_0 [1 + \alpha(r/r_e - 1)] e^{-\alpha(r/r_e - 1)}, \quad (15)$$

where $\alpha = \sqrt{9\Omega_0 B/E_0}$, and r, E_0, Ω_0, B, r_e are the nearest-neighbor distance, cohesive energy, equilibrium atomic volume, the bulk modulus, and the equilibrium-nearest neighbor distance, respectively. It is generally found that the EAM potentials which exactly follow Rose’s EOS [Eq. (15)] underestimate energies at high pressures.³¹ We have therefore modified Eq. (15) to allow for a more accurate fit to energies at high pressures. The modified equation has the form

$$E(r) = -E_0 \left[1 + \alpha x + \beta \alpha^3 x^3 \frac{2x+3}{(x+1)^2} \right] e^{-\alpha x}, \quad (16)$$

with $x = (r/r_e - 1)$. The parameter β in this equation is related to the pressure derivative of the bulk modulus at equilibrium as $B'_0 = \frac{2}{3}\alpha + 6\alpha\beta + 2$. This modification does not alter the exact fitting of the potential to E_0, r_e and B but provides a way to achieve an accurate fit to the experimental pressure-volume relation by adjusting the value of β .

C. EAM potential for Ti

Titanium has the hcp structure at $T = 0$ (α -Ti phase). For hcp metals, an EAM potential can only be fitted to elastic constants C_{ij} if the relation $(3C_{12} - C_{11})/2 > (C_{13} - C_{44})$ is satisfied.³⁵ Fortunately, this relation holds for α -Ti.

In the present EAM potential for Ti, the electron density function is described by

$$\rho(r) = \left[Ae^{-\alpha_1(r-r_0)^2} + e^{-\alpha_2(r-r'_0)} \right] \psi\left(\frac{r-r_c}{h}\right), \quad (17)$$

where the cutoff function $\psi(x)$ is given by Eq. (13) with the fitting parameters $A, \alpha_1, \alpha_2, r_0, r'_0, r_c$, and h . One of the parameters is fixed by the normalization condition $\bar{\rho} = 1$ at equilibrium.

The pair interaction function is represented by

$$\Phi(r_{ij}) = \psi\left(\frac{r-r_c}{h}\right) \left\{ V_0 e^{-\beta_1 r_1} + V'_0 \left[e^{-2\beta_2(r-r'_1)} - 2 e^{\beta_2(r-r'_1)} \right] + \delta \right\}, \quad (18)$$

where $V_0, V'_0, \beta_1, \beta_2, r_1, r'_1$, and δ are fitting parameters. The embedding energy function is expressed as a polynomial:

$$\begin{aligned} F(\bar{\rho}) = & F_0 + \frac{1}{2} F_2 (\bar{\rho} - 1)^2 + q_0 (\bar{\rho} - 1)^3 \\ & + \sum_{i=1}^3 B_i (\bar{\rho} - 1)^{i+3}. \end{aligned} \quad (19)$$

Here F_0 and F_2 are the embedding energy and its second derivative at equilibrium, respectively. These can be expressed in terms of the experimental values of E_0 , B , and Ω_0 :

$$F_0 = E_0 - \frac{1}{2} \sum_j N_j \Phi_j$$

and

$$\frac{1}{2} \sum_j N_j \Phi_j'' R_j^2 + F_2 \left(\sum_j N_j \rho_j R_j \right)^2 = 9B\Omega_0,$$

where j runs over coordination shells, N_j is the number of atoms on the j -th coordination shell of radius R_j , while Φ_j and Φ_j'' are the pair interaction energy and its second derivative evaluated at R_j . The coefficients q_0 and B_i ($i \leq 3$) in Eq. (19) are fitting parameters. The parameter q_0 was adjusted to ensure that the embedding energy vanishes when the electron

density goes to zero, that is, $F(0) = 0$. This requirement leads to the following expression for q_0 :

$$q_0 = F_0 + \frac{F_2}{2} + B_1 - B_2 + B_3. \quad (20)$$

During the optimization of fitting parameters, the energy of the hcp structure was required to approximately follow the Rose's EOS [Eq. (15)] in the neighborhood of equilibrium. This was achieved by adding to the objective function the mean-squared deviation of the energy from Eq. (15) at several points near the equilibrium.

D. The cross potential Ti-Al and the fitting procedure

Once the EAM potentials for Al and Ti are obtained, the cross potential representing the interactions between Ti and Al atoms was constructed by employing the parametrization given by Eq. (14). The transformation coefficients s_{Al} , g_{Ti} , and g_{Al} [see Eqs. (3)-(11)] were used as additional adjustable parameters.

It should be mentioned that the specific analytical forms of the potential functions adopted in this work were found by trying a number of different forms and selecting those which provided a better accuracy of fitting with less parameters. The optimized values of the fitting parameters are listed in Table I. The potential functions are plotted in Fig. 1 in the effective pair format^{31,57} with respect to γ -TiAl. These functions are available in the tabulated form on Internet⁵⁹ or from the authors upon request. The cutoff radii of atomic interactions in Al, Ti, and TiAl are 6.72, 5.19, and 5.77 Å, respectively. The fitting procedure involves the total of 39 independent fitting parameters.

III. TESTS AND APPLICATIONS OF THE POTENTIALS

A. Aluminum

The accuracy of the fitted EAM potential for Al can be adjudged from Table II, wherein the basic lattice properties, elastic constants, vacancy formation and migration energies, surface energies, and the stacking fault energy predicted by the potential are compared with their experimental values. We have also included the results obtained with our previous EAM potential for Al,²⁸ which we hereafter refer to as MFMP. The results obtained with the new

EAM potential are in good agreement with their experimental counterparts. The calculated vacancy formation energy E_v^f and migration energy E_v^m , which are important for studying point defect diffusion, are well reproduced. The calculated vacancy formation volume Ω_v^f compares well with the one obtained with the MFMP potential as well as with experimental data.⁶⁰ The predicted intrinsic stacking fault (γ_{SF}) energy is on the lower end of the range of experimental values while the *ab initio*^{101,102} calculations yeilds a higher value of 166 mJ/m² . The calculated symmetrical twin boundary (γ_T) energy is in good agreement with its experimental counterpart. The unstable stacking fault energy is underestimated with respect to the *ab initio*^{101,102} value of 220 mJ/m² . The surface energies are underestimated in comparison with experiment, which is a general characteristic of EAM potentials.

The structural energy differences for Al, given in Table III, reproduce *ab-initio* energies reasonably accurately. The EAM potential predicts the c/a ratio of the hcp structure to be 1.63 in good agreement with the optimized value of 1.645 obtained by the LAPW calculations. In agreement with earlier findings,²⁸ bcc Al is mechanically unstable ($C_{11} < C_{12}$) and transforms to the fcc structure upon c/a relaxation. The sc structure is also mechanically unstable with $C_{44} < 0$. A comparison of the EOS's of various crystalline structures of Al calculated with the EAM potential and by the LAPW method is presented in Fig. 2. The EAM curves are seen to agree with the LAPW results fairly well. The agreement is particularly good for the bcc and fcc structures over a large range of volumes, but tends to worsen for more open structures.

As was mentioned in Section II B, the Al potential was fit to the experimental $P(V)$ relation by adjusting the parameter β in the generalized EOS, Eq. (16). The optimized value of $\beta = 0.00489$ provides an excellent agreement with experimental data up to pressures of about 700 GPa, as illustrated in Fig. 3. In contrast, the standard Rose's EOS ($\beta = 0$) underestimates the pressures under strong compressions. Note that both equations share the same values of E_0 , B and a_0 . The excellent fit to high pressure data makes the potential useful for simulating shock waves, sputter deposition, and other processes involving a close approach of atoms.

Thermal expansion of Al was studied within the temperature range of 5-1000 K. The calculated thermal expansion factors at selected temperatures are given in Table IV. They were obtained using a 864-atom supercell by two different methods. In the first method, the free energy of the crystal was minimized as a function of volume in the quasiharmonic

approximation.⁶¹ This method includes quantum-mechanical effects such as zero-point vibrations and should yield more accurate values of the thermal expansion factor at low temperatures. However, it may not be very accurate at high temperature where the anharmonic effects become significant. The second type of calculation was carried out by the Metropolis Monte Carlo method.^{61,62} This method is based on classical mechanics and fully incorporates anharmonic effects. It is therefore more adequate for thermal expansion calculations at high temperatures. As can be seen from Table IV, the MC results are quite close to experimental data at high temperatures.

Overall, the EAM potential developed here provides a good description of a wide range of Al properties. Despite the existence of other high-quality EAM potentials for Al in the literature,^{23,28,34} we chose not to re-use one of them but rather generate a new potential so that to have all potential functions for the Ti-Al system created by the same methodology. We also used this work as an opportunity to address some weak points of previous potentials. For example, even though the MFMP potential²⁸ demonstrates a better agreement with experiment for some of the properties listed in Table II, the present potential describes the thermal expansion and high-pressure behavior of Al more accurately. The present potential is also based on a larger set of *ab-initio* data and should be better transferable to configurations away from equilibrium. It should also be mentioned that the use of smooth analytical functions in this work makes the potential more robust in comparison with the cubic-spline parameterization applied in Ref. 28.

B. Titanium

Equilibrium lattice properties, vacancy characteristics, as well as stacking fault and surface energies in Ti computed using the present EAM potential are compared with experimental data in Table V. We have also included the results obtained with the EAM potential developed by Fernandez *et al.*,³⁷ which will be referred to as FMP. The latter is an improved version of the potential proposed in Ref. 35. Although our potential was not fitted to the c/a ratio exactly, the predicted value of 1.585 is in a good agreement with the experimental value of 1.588. The elastic constants are also reproduced reasonably well.

The vacancy formation energy E_v^f was fitted to the target value of 1.85 eV. The experimental value of E_v^f reported by Shestopal⁶³ is 1.55 eV, more recent positron annihilations

measurements⁶⁴ give $E_v^f = 1.27$ eV, while the *ab-initio* linearized muffin-tin orbital method (LMTO) method⁶⁵ yields a much higher value of 2.14 eV. We therefore opted to fit to an intermediate value of 1.85 eV, which after the relaxation decreased to 1.83 eV. The vacancy migration energy E_v^m was calculated using the nudged elastic band method.⁶⁶ In the hcp lattice with a nonideal c/a ratio, the basal and non-basal vacancy jumps are not identical. The calculated values of E_v^m for the basal and non-basal jumps are 0.80 eV and 0.83 eV, respectively. The FMP potential gives smaller values of 0.51 eV and 0.48 eV, respectively. While the experimental value of the vacancy formation energy is rather uncertain, the experimental activation energy Q of self-diffusion in α -Ti, which is the sum of E_v^f and E_v^m , has been measured fairly accurately.⁶⁷ For self-diffusion perpendicular to the c axis, the experimental value is $Q = 3.14$ eV. The present EAM potential predicts $Q = 2.62$ eV, while the FMP potential gives a lower value of 2.02 eV.

There are three stacking faults on the basal plane in α -Ti, which are deviations from the normal stacking sequence $ABABAB$ of closed packed planes in the hcp structure.^{68,69} The intrinsic fault I_1 is formed by a removal of one hexagonal layer followed by a $\frac{1}{3} < 10\bar{1}0 >$ translation of all atoms above this fault. The resultant stacking sequence is

$$I_1 : ABAB|C\bar{C}C\bar{C},$$

where the vertical bar indicates the position of the fault. The intrinsic stacking fault I_2 is created by a $\frac{1}{3} < 10\bar{1}0 >$ slip:

$$I_2 : ABAB|CACAC.$$

The extrinsic stacking fault E result from the insertion of an extra hexagonal plane into the normal stacking sequence:

$$I_E : ABAB|C|ABAB.$$

The calculated relaxed stacking fault energies (Table V) compare well with those obtained with the FMP potential. The experimental value of the I_2 fault energy is about 300 mJ/m² and is considered to be a rough estimate. Both EAM potentials underestimate this experimental value. All our efforts to obtain a higher γ_{I_2} value during the fitting of the present potential did not have much success. In fact, any attempt to raise γ_{I_2} above 66 mJ/m² resulted in a deterioration of other properties, which gave us an indication that higher stacking fault energies may be beyond the capabilities of the EAM. Note, however, that the

EAM-predicted stacking fault energies follow the expected relation:⁶⁸ $\gamma_E \approx \frac{3}{2}\gamma_{I_2} \approx 3\gamma_{I_1}$. The limited success in fitting to higher stacking fault energies is likely to be due to the directional component of bonding in Ti owing to d electrons. The covalent nature of bonding cannot be described by the central-force-based EAM model. More rigorous parameter-based methods such as the modified EAM,^{36,70} bond order potentials^{71,72,73} or the tight-binding method,⁷⁴ which include angular-dependent interactions, may give higher stacking fault energies.

The predicted value of the (0001) surface energy, 1725 mJ/m², slightly underestimates the experimental value. This is again consistent with the general trend of the EAM to underestimate surface energies. The FMP potential yields an even smaller value of 1439 mJ/m², whereas the *ab-initio* surface energies, 2100 mJ/m² (Ref. 75) and 1920 mJ/m² (Ref. 76), overestimate the experimental value.

The LAPW and the EAM energies of various crystal structures of Ti relative to the hcp structure are reported in Table VI. We note that the LAPW calculations predict the omega structure to be the ground state, with the hcp energy being 0.06 eV/atom higher. We have, therefore, excluded the omega structure from the fitting procedure. Overall, both EAM potentials yield similar energy differences between the structures, with the present potential performing somewhat better. Both potentials predict the hcp structure to be more stable than the omega structure in agreement with experiment. In Fig. 4, the EOS's of the hcp, fcc, bcc, and the sc structures of Ti calculated with the present EAM potential are compared with the LAPW results. The agreement between the two calculation methods is good for the close-packed structures but becomes poorer for the low coordinated sc structure. In the latter case, however, the present EAM potential is closer to the LAPW data than the FMP potential.

The linear thermal expansion of Ti was calculated within the quasiharmonic approximation and by the MC method using a supercell with 800 atoms. The c/a ratio was kept fixed at its equilibrium $T = 0$ value during the calculations. The obtained values of the thermal expansion factor for selected temperatures are reported in Table VII. The agreement with experimental data⁷⁷ for polycrystalline Ti is reasonable. The FMP potential gives a poorer agreement with experiment. For example, at 293 K the FMP potential gives the quasiharmonic linear thermal expansion of 1.35% while the experimental value is 0.15%.

C. Intermetallic compound γ -TiAl

The physical properties of γ -TiAl obtained with the present EAM potential are summarized in Table VIII. The lattice constant and the cohesive energy are reproduced accurately. The c/a ratio is correctly predicted to be larger than unity and is in good agreement with the experimental value. The elastic constants are in a reasonable agreement with experiment, the root-mean-squared deviation for elastic constants being about 22%. We note that the negative signs of the two Cauchy pressures, $(C_{12} - C_{66})$ and $(C_{13} - C_{44})$, are not reproduced by the present potential, nor are they reproduced by previous EAM-type potentials. The negative Cauchy pressures in TiAl are caused by the directional component of bonding and cannot be described by the EAM. Table VIII also includes the numbers calculated with the Farkas potential^{38,78} as well as with the P_2 potential constructed by Simmons *et al.*²¹ The respective root-mean-squared deviations of the elastic constants from experimental data are 45% and 28%.

The planar defect energies in γ -TiAl are summarized in Table IX. They were calculated using supercells with an effective cubic lattice with the lattice parameter $a = (a_0^2 c_0)^{1/3}$ and without volume relaxation. Since the cohesive energy of the equilibrium tetragonal lattice was used as a reference in the calculations, the resultant fault energies can be slightly overestimated. For the superlattice intrinsic stacking fault (SISF), the EAM value of 173 mJ/m² is slightly higher than the experimental value of 140 mJ/m². There have been a number of *ab-initio* calculations of the SISF energy with results scattered over the range of 90-172 mJ/m². For the complex stacking fault (CSF) energy we obtain the value of 299 mJ/m² well bracketed between *ab-initio* results. Experimental data for the CSF energy are not available. The calculated value of the antiphase boundary (APB) energy, 266 mJ/m², is also in a good agreement with the experimental value of 250 mJ/m². The *ab-initio* APB energies are scattered over the wide range 510-670 mJ/m². The hierarchy of planar fault energies in γ -TiAl was investigated by Wiezorek and Humphreys.⁷⁹ According to their preliminary computational results, this hierarchy in Ti-54at%Al is $\gamma_{CSF} > \gamma_{APB} > \gamma_{SISF}$. The present EAM potential predicts the same ordering. On the other hand, *ab-initio* calculations with the linearized Korringa-Kohn-Rostoker (LKKR) method⁸⁰ and the full potential LAPW (FLAPW) method⁸¹ give the $\gamma_{APB} > \gamma_{CSF} > \gamma_{SISF}$ ordering. More recent calculations by Ehmann and Fähnle by the LAPW method including local atomic relaxations are

consistent with the latter ordering of the stacking fault energies. The discrepancy between the experimental data and EAM calculations, on one hand, and *ab-initio* calculations, on the other hand, originates primarily from the high APB energy delivered consistently by *ab-initio* methods. The low APB energy observed experimentally may reflect the local disorder near the APB taking place due to the off-stoichiometry and/or temperature effects. The similarly low APB energy predicted by the present EAM potential can lead to a good agreement between atomistic simulations and experiment.

Simmons *et al.*²¹ succeeded in generating a set of EAM potentials for γ -TiAl fit to high APB energies comparable to *ab-initio* values, but their potentials give $c/a < 1$ in contradiction to experimental data. When generating our potential we could also achieve higher γ_{APB} values at the expense of $c/a < 1$, but could never increase γ_{APB} above 266 mJ/m² while keeping $c/a > 1$ and maintaining a good quality of fit to other properties. We believe that the underestimation of the APB energy is another intrinsic limitation of the central-force EAM as applied to γ -TiAl. Farkas³⁸ constructed a potential that gives $\gamma_{APB} > \gamma_{CSF}$ while $c/a > 1$. However, some of the elastic constants predicted by that potential are in a poor agreement with experimental data, especially C_{13} and C_{33} (cf. Table VIII). The potential also gives a discontinuous temperature dependence of the quasiharmonic thermal expansion, with unrealistically large values at high temperatures.

The *EV* curves computed with the present EAM potential and by the LAPW method are presented in Fig. 5. The agreement between the two calculation methods is good for the L1₀ structure. The difference between the two curves for the B2 and B1 structures is presumably due to the limited accuracy of the EAM method to describe the open structures. The formation energies for different structures of TiAl (relative to fcc Al and hcp Ti) calculated by the LAPW method and with the present EAM potential are presented in Table X. For comparison, experimental and *ab-initio* results available in the literature have also been included in the Table. The formation energies obtained with the present EAM potential are in good agreement with the corresponding experimental and *ab-initio* energies. The $\mathfrak{l}10$ structure is correctly produced to be the ground state. We note the *B2* and *B32* structures are unstable with respect to the c/a optimization. In particular, the *B2* structure transforms to the equilibrium $\mathfrak{l}10$ phase upon c/a relaxation.

For Ti₃Al, the EAM potential correctly predicts the DO₁₉ structure to be the equilibrium ground state of Ti₃Al (Table X). The lattice constants, cohesive energy, and the

elastic constants of $D0_{19}$ - Ti_3Al are given in Table XI. We emphasize that none of these properties were included in the potential fit. The observed agreement with experimental data demonstrates a good transferability of our potential.

The EAM potential was also applied to investigate the Al_3Ti compound. Experimentally, the equilibrium structure of Al_3Ti is DO_{22} . The present EAM potential predicts the $L1_2$ structure to be 0.01 eV lower in energy than the DO_{22} structure, suggesting that the potential may not suitable for simulating the Al_3Ti compound.

Thermal expansion factors of γ - $TiAl$ calculated within the quasiharmonic approximation and by the Monte Carlo method are presented in Table XII. The calculated values are in agreement with those estimated from Fig. 4 in Ref. 82.

The energy along the Bain path between the tetragonal γ - $TiAl$ structure and the $B2$ structure was calculated by the EAM and LAPW methods. Starting from the equilibrium tetragonal γ - $TiAl$ structure, the c/a ratio was varied by keeping the volume constant. The energy change during the transformation is plotted in Fig. 6 as a function of the deformation parameter X defined by $c/a = X(c_0/a_0)$. The EAM energies are observed to closely follow the LAPW energies along the path. This agreement confirms a good transferability of the present EAM potential.

Point defect properties play an important role in the atomic disorder and diffusion in γ - $TiAl$. The $TiAl$ lattice supports two types of vacancy (V_{Ti} and V_{Al}) and two types of antisite defects (Ti atom on the Al sublattice, Ti_{Al} , and Al atom on the Ti sublattice, Al_{Ti}).¹² The so-called “raw” formation energies and entropies¹² of the defect formation have been calculated with the present EAM potential using the molecular statics method for the energies and the quasiharmonic approximation for the entropies.

When analyzing point defects in ordered compounds it is more convenient to deal with hypothetical composition-conserving defect complexes rather than individual defects.^{12,83,84,85} It should be emphasized that the defects are grouped into complexes conceptually and not physically. The complexes are assumed to be totally dissociated and interactions between their constituents are neglected. The advantage of dealing with composition-conserving complexes is that all reference constants involved in their energies and entropies cancel out. This allows us to directly compare results obtained by different calculation methods. The complex energies and entropies can be expressed in terms of the “raw” energies ϵ_d and entropies s_d , $d = V_{Ti}, V_{Al}, Ti_{Al}, Al_{Ti}$.¹² The expressions for some of the complex energies are

given in Table XIII. Similar expressions hold for the complex entropies, except that the cohesive energy E_0 should be replaced by the perfect lattice entropy per atom. Table XIII summarizes the results of the EAM calculations for several defect complexes and compares them with the *ab-initio* energies reported by Woodward *et al.*⁸⁶ The agreement between the two calculation methods is reasonable. We emphasize again that point defect properties of γ -TiAl were not included in the potential fit.

Using the complex energies and entropies, the equilibrium defect concentrations have been calculated as functions of the bulk composition around the stoichiometry within the lattice gas model of non-interacting defects.^{12,83,84,85} Fig. 7 shows the calculation results for $T = 1000$ K. We see that all compositions are strongly dominated by antisite defects. This observation is well consistent with the experimentally established fact that γ -TiAl is an antisite disorder compound.^{87,88,89} The vacancy concentrations are several orders of magnitude smaller than antisite concentrations. In the stoichiometric composition, most of the vacancies reside on the Ti sublattice. All these features have been observed at all temperatures in the range 800-1200 K.

IV. SUMMARY

EAM potentials have been developed for Al, α -Ti and γ -TiAl by fitting to a database of experimental data and *ab-initio* calculations. The potentials have been tested against other experimental and *ab-initio* data not included in the fitting database. The *ab-initio* structural energies for Ti were calculated previously,⁴⁴ while those for Al and Ti-Al compounds have been generated in this work. All these calculations employed the full-potential LAPW method within the GGA approximation. Besides serving for the development of the EAM potentials, the obtained *ab-initio* energies are also useful as reference data for the Ti-Al system.

The Al potential is fit to the target properties very accurately and has demonstrated a good performance in the tests. It has certain advantages over the previously developed potential,²⁸ particularly with respect to the lattice thermal expansion and the pressure-volume relation under large compressions. The fit of the Ti potential is less successful, presumably because of the directional component of interatomic bonding that is not captured by the central-force EAM model. In particular, the potential underestimates the stacking

fault energies on the basal plane. Further improvements of the potential do not appear to be possible within the EAM. This potential can be viewed as a supporting potential for the Ti-Al system, but we also believe that it can be useful in atomistic simulations in pure Ti where subtle details of atomic interactions may not be critical. Since the potential is fit reasonably well to the elastic constants, thermal expansion factors and the vacancy formation energy, it can be employed for modeling diffusion and creep in large systems that are not accessible by more accurate, yet slower, *ab-initio* methods.

For the γ -TiAl compound, the potential developed here reproduces reasonably well the basic lattice properties, planar fault energies, as well as point defect characteristics. The fit to the elastic constants is better than with previous potentials. However, the negative Cauchy pressures in γ -TiAl have not been reproduced by the present nor previous EAM potentials. The planar fault energies calculated with the potential are in a good agreement with experiment, but the APB energy is lower than all *ab-initio* values. The fit to *ab-initio* energies of alternative structures of TiAl enhances the transferability of the potential to configurations away from equilibrium. This fact is verified by the good agreement between the EAM and LAPW energies along the Bain transformation path. The potential also correctly predicts the equilibrium DO_{19} structure of Ti_3Al and gives a fairly good agreement with experiment for the cohesive energy, lattice parameters, and elastic constants of this compound. The point defect energies and entropies in γ -TiAl calculated with the potential are in agreement with the antisite disorder mechanism established for this compound experimentally. We emphasize that neither the Bain path nor any information on Ti_3Al or point-defect properties in γ -TiAl were included in the fitting database. This success of the proposed potential points to its ability to describe atomic interactions in the Ti-Al system on a reasonable quantitative level. The potential should be suitable for large-scale atomistic simulations of plastic deformation, fracture, diffusion, and other processes in γ -TiAl. At the same time we acknowledge that more rigorous models, particularly those including angular-dependent interactions, are needed for addressing the negative Cauchy pressures, high APB energy, and other properties of γ -TiAl that lie beyond the capabilities of the EAM.

Acknowledgments

We would like to thank A. Suzuki for helpful discussions and assistance with some of the calculations. We are grateful to M. J. Mehl and D. A. Papaconstantopoulos for making the LAPW energies for Ti available to us prior to publication,⁴⁴ as well as for helpful comments on the manuscript. We are also grateful to R. Pasianot for sending us the potential of Ref. 37 in a convenient format, and for very useful comments on EAM for hcp metals. This work was supported by the US Air Force Office of Scientific Research through Grant No. F49620-01-0025.

* Electronic address: rzope@scs.gmu.edu, ymishin@gmu.edu

¹ Y. W. Kim, J. Metals **46**(7), 30 (1994).

² F. Appel, P. A. Beaven, and R. Wagner, Acta. Metall. Mater. **41**, 1721 (1993).

³ M. Yamaguchi, H. Inui, K. Koshoda, M. Matsumorto, and Y. Shirai, in *High-Temperature Ordered Intermetallic Alloys VI*, edited by J. Horton (Materials Research Society, Pittsburg, 1996), vol. 364.

⁴ M. Yamaguchi, H. Inui, and K. Ito, Acta Mater **48**, 307 (2000).

⁵ L. Hsiung, T. Nieh, B. W. Choi, and J. Wadsworth, Mater. Sci. and Eng. A **329**, 637 (2002).

⁶ F. Appel, Mater. Sci. and Eng. A **317**, 115 (2001).

⁷ O. N. Mryasov, Y. N. Gornostyrev, and A. J. Freeman, Phys. Rev. B **58**, 11927 (1998).

⁸ J. P. Simmons, S. I. Rao, and D. M. Dimiduk, Phil. Mag. Lett **77**, 327 (1998).

⁹ W. J. Zhang, B. V. Reddy, and S. C. Deevi, Scripta Materialia **45**, 645 (2001).

¹⁰ C. Fu and M. Yoo, Intermetallics **1**, 59 (1993).

¹¹ T. Ikeda, H. Kadowaki, H. Nakajima, H. Inui, M. Yamaguchi, and M. Koiwa, Mater. Sci. and Eng. A **312**, 155 (2001).

¹² Y. Mishin and C. Herzog, Acta. mater. **48**, 589 (2000).

¹³ C. L. Fu, J. Zou, and M. H. Yoo, Scripta Meallurgica et Materialia **33**, 885 (1995).

¹⁴ T. Hong, T. J. Watson-Yang, X. Q. Guo, A. J. Freeman, T. Oguchi, and J. Xu, Phys. Rev. B **43**, 1940 (1991).

¹⁵ T. Hong, T. J. Watson-Yang, A. J. Freeman, T. Oguchi, and J. Xu, Phys. Rev. B **41**, 12 462

(1990).

- ¹⁶ C. L. Fu, *J. Mater. Res.* **5**, 971 (1990).
- ¹⁷ M. S. Daw and M. I. Baskes, *Phys. Rev. Lett.* **50**, 1285 (1983).
- ¹⁸ M. S. Daw and M. I. Baskes, *Phys. Rev. B* **29**, 6443 (1984).
- ¹⁹ M. S. Daw, S. M. Foiles, and M. I. Baskes, *Mater. Sci. Rep.* **9**, 251 (1993).
- ²⁰ M. W. Finnis and J. E. Sinclair, *Philos. Mag. A* **50**, 45 (1984).
- ²¹ J. P. Simmons, S. I. Rao, and D. M. Dimiduk, *Philos. Mag. A* **75**, 1299 (1997).
- ²² V. Paidar, L. G. Wang, M. Sob, and V. Vitek, *Modell. Simul. Mater. Sci. Eng.* **7**, 369 (1999).
- ²³ F. Ercolessi and J. B. Adams, *Europhys. Lett.* **26**, 583 (1994).
- ²⁴ D. T. Kulp, G. J. Ackland, M. Sob, V. Vitek, and T. Egami, *Model. Simul. Mater. Sci. Eng.* **1**, 315 (1993).
- ²⁵ X. Y. Liu, J. B. Adams, F. Ercolessi, and J. A. Moriarty, *Model. Simul. Mater. Sc.* **4**, 293 (1996).
- ²⁶ A. Landa, P. Wynblatt, A. Girshick, V. Vitek, A. Ruban, and H. Skriver, *Acta. Mater.* **46**, 3027 (1998).
- ²⁷ L. G. Ferreria, V. Ozolins, and A. Zunger, *Phys. Rev. B* **60**, 1687 (1999).
- ²⁸ Y. Mishin, D. Farkas, M. J. Mehl, and D. A. Papaconstantopoulos, *Phys. Rev. B* **59**, 3393 (1999).
- ²⁹ A. B. Belonoshko, R. Ahuja, O. Eriksson, and B. Johansson, *Phys. Rev. B* **61**, 3838 (2000).
- ³⁰ Y. Mishin, M. J. Mehl, D. A. Papaconstantopoulos, A. F. Voter, and J. D. Kress, *Phys. Rev. B* **63**, 224106 (2001).
- ³¹ Y. Mishin, M. J. Mehl, and D. A. Papaconstantopoulos, *Phys. Rev. B* **65**, 224114 (2002).
- ³² M. I. Baskes, M. Asta, and S. G. Srinivasan, *Philos. Mag. A* **81**, 991 (2001).
- ³³ A. F. Voter and S. P. Chen, *MRS Symp. Proc.* **82**, 175 (1987).
- ³⁴ U. Hansen, P. Vogl, and V. Fiorentini, *Phys. Rev. B* **60**, 5055 (1999).
- ³⁵ R. Pasianot and E. J. Savino, *Phys. Rev. B* **45**, 12704 (1992).
- ³⁶ M. I. Baskes and R. A. Johnson, *Modell. Simul. Mater. Sci. Eng.* **2**, 147 (1994).
- ³⁷ J. R. Fernandez, A. Monti, and R. Pasianot, *J. Nucl. Mater.* **229**, 1 (1995).
- ³⁸ D. Farkas, *Modell. Simul. Mater. Sci. Eng.* **2**, 975 (1994).
- ³⁹ S. I. Rao, C. Woodward, and T. A. Parthasarathy, *Mater. Res. Soc. Symp. Proc.* **213**, 125 (1991).

⁴⁰ S. I. Rao, C. Woodward, J. Simmons, and D. Dimiduk, Mater. Res. Soc. Symp. Proc. **364**, 129 (1995).

⁴¹ D. Chen, M. Yan, and Y. F. Liu, Scripta Materialia **40**, 913 (1999).

⁴² T. Wang, B. Wang, X. Ju, Q. Gu, Y. Wang, and F. Gao, Chin. Phys. Lett. **18**, 361 (2001).

⁴³ V. Paidar, L. G. Wang, M. Sob, and V. Vitek, Modell. Simul. Mater. Sci. Eng. **7**, 369 (1999).

⁴⁴ M. J. Mehl and D. A. Papaconstantopoulos, Europhys. Lett. **60**, 248 (2002).

⁴⁵ R. E. Watson and M. Weinert, Phys. Rev. B **58**, 5981 (1998).

⁴⁶ O. K. Anderson, Phys. Rev. B **12**, 3060 (1975).

⁴⁷ S. H. Wei and H. Krakauer, Phys. Rev. Lett. **55**, 1200 (1985).

⁴⁸ D. J. Singh, *Planewaves, Pseudopotentials and the LAPW Method* (Kluwer Academic, Boston, 1994).

⁴⁹ P. Hohenberg and W. Kohn, Phys. Rev. B **136**, 1940 (1964).

⁵⁰ W. Kohn and L. J. Sham, Phys. Rev. A **140**, 1133 (1965).

⁵¹ R. G. Parr and W. Yang, *Density Functional Theory of Atoms and Molecules* (Oxford, New York, 1989).

⁵² P. Blaha, K. Schwarz, G. Madsen, D. Kvasnicka, and J. Luitz, *WIEN2K* (Technical University of Vienna, 2002).

⁵³ J. P. Perdew, in *Electronic Structure of Solids '91*, edited by P. Ziesche and H. Eschrig (Akademie-Verlag, Berlin, 1991).

⁵⁴ J. P. Perdew, J. A. Chevary, S. H. Vosko, K. A. Jackson, M. R. Pederson, D. J. Singh, and C. Fiolhais, Phys. Rev. B **46**, 6671 (1992).

⁵⁵ J. P. Perdew, J. A. Chevary, S. H. Vosko, K. A. Jackson, M. R. Pederson, D. J. Singh, and C. Fiolhais, Phys. Rev. B **48**, 4978(E) (1993).

⁵⁶ J. P. Perdew, K. Burke, and E. Ernzerhof, Phys. Rev. Lett. **77**, 3865 (1996).

⁵⁷ R. A. Johnson, Phys. Rev. B **39**, 12 554 (1989).

⁵⁸ J. H. Rose, J. R. Smith, F. Guinea, and J. Ferrante, Phys. Rev. B **29**, 2963 (1984).

⁵⁹ The potential functions are available in the tabulated form at <http://cst-www.nrl.navy.mil/bind/eam>.

⁶⁰ R. M. Emrick and P. B. McArdle, Phys. Rev. **188**, 1156 (1969).

⁶¹ S. M. Foiles, Phys. Rev. B **49**, 14930 (1994).

⁶² S. M. Foiles and J. B. Adams, Phys. Rev. B **40**, 5909 (1989).

⁶³ V. O. Shestopal, Sov. Phys. Solid **7**, 2798 (1966).

⁶⁴ E. Hashimoto, E. A. Smirnov, and T. Kino, J. Phys. F **14**, L215 (1984).

⁶⁵ O. L. Bacq, F. Willaime, and A. Pasturel, Phys. Rev. B **59**, 8508 (1999).

⁶⁶ H. Jonsson, G. Mills, and K. W. Jacobsen, in *Classical and Quantum Dynamics in Condensed Phase Simulations*, edited by B. J. Berne, G. Ciccotti, and D. G. Coker (World Scientific, Singapore, 1998).

⁶⁷ M. Koppers, C. Herzig, M. Friesel, and Y. Mishin, Acta. Mater. **45**, 4181 (1997).

⁶⁸ D. Hull and D. J. Bacon, *Introduction to Dislocations* (Pergamon Press, Oxford, 1989).

⁶⁹ J. P. Hirth and J. Lothe, *Theory of dislocations* (Wiley International, 1982).

⁷⁰ M. I. Baskes, Phys. Rev. B **46**, 2727 (1992).

⁷¹ M. Akoi, Phys. Rev. Lett. **71**, 3842 (1993).

⁷² M. Akoi and D. G. Pettifor, Mater. Sci and Eng. A **176**, 19 (1994).

⁷³ A. Girshick, A. M. Bratkovsky, D. G. Pettifor, and V. Vitek, Philos. Mag. A **77**, 981 (1998).

⁷⁴ M. J. Mehl and D. A. Papaconstantopoulos, Phys. Rev. B **54**, 4519 (1996).

⁷⁵ F. R. de Boer, R. Boom, W. C. M. Mattens, A. R. Moedema, and A. Niessen, *Cohesion in Metals* (North-Holland, Amsterdam, 1988).

⁷⁶ W. R. Tyson and W. R. Miller, Surf. Sci. **62**, 267 (1977).

⁷⁷ Y. S. Touloukian, R. K. Kirby, R. E. Taylor, and P. D. Desai, eds., *Thermal Expansion: Metallic Elements and Alloys*, vol. 12 (Plenum, New York, 1975).

⁷⁸ The version of the potential available to us does not reproduce the elastic constant reported in Table 2 of Ref. 38, whereas all other properties are reproduced exactly.

⁷⁹ J. Wiezorek and C. J. Humphreys, Scripta Metallurgica et Materialia **33**, 451 (1995).

⁸⁰ C. Woodward, J. M. MacLauren, and S. I. Rao, J. Mater. Res. **7**, 1735 (1992).

⁸¹ C. L. Fu and M. H. Yoo, Phil. Mag. Lett **62**, 159 (1990).

⁸² M. Zupan and K. J. Hemker, Mater. Sci. and Eng. A**319-321**, 810 (2001).

⁸³ M. Hagen and M. W. Finnis, Philos. Mag. A **77**, 447 (1998).

⁸⁴ P. A. Korzhavyi, A. V. Ruban, A. Y. Lozovoi, Y. K. Vekilov, I. A. Abrikosov, and B. Johansson, Phys. Rev. B **61**, 6003 (2000).

⁸⁵ B. Meyer and M. Fähnle, Phys. Rev. B **59**, 6072 (1999).

⁸⁶ C. Woodward, S. Kajihara, and L. H. Yang, Phys. Rev. B **57**, 13459 (1998).

⁸⁷ M. J. Elliot and W. Rostoker, Acta. Metall. **2**, 884 (1954).

88 U. Brossmann, R. Wurschum, K. Badura, and H. E. Schaefer, Phys. Rev. B **49**, 6457 (1994).

89 Y. Shirai and M. Yamaguchi, Mater. Sci Eng. A **2**, 975 (1992).

90 Y. Wang, D. Chen, and X. Zhang, Phys. Rev. Lett. **84**, 3220 (2000).

91 W. J. Nellis, J. A. Moriarty, A. C. Mitchell, M. Ross, R. G. Dandrea, N. W. Ashcroft, N. C. Holmes, and G. R. Gathers, Phys. Rev. Lett. **60**, 1414 (1988).

92 Measurements from Los Alamos Series on Dynamic Materials Properties. Last Shock Hugoniot Data, S.P. March, ed. (1980), p. 195 (Al alloy 1100).

93 C. Kittel, *Introduction to Solid State Physics* (Wiley-Interscience, New York, 1996).

94 R. C. Weast, ed., *Handbook of Chemistry and Physics* (CRC, Boca Raton, FL, 1984).

95 G. Simons and H. Wang, *Single Crystal Elastic Constants and Calculated Aggregate Properties* (MIT press, Cambridge, Massachusetts, 1977).

96 H. Schaefer, R. Gugelmeier, M. Schmolz, and A. Seeger, Mater. Sci. Forum **15,16,17,18**, 111 (1987).

97 R. W. Balluffi, J. Nucl. Mater. **69-70**, 240 (1978).

98 L. E. Murr, *Interfacial Phenomena in Metals and Alloys* (Addison-Wesley, Reading, MA, 1975).

99 Rautioaho, Phys. Status. Solidi B **23**, 611 (1971).

100 K. H. Westmacott and R. L. Peck, Philos. Mag. **23**, 611 (1971).

101 Y. Sun and E. Kaxiras, Philos. Mag. A **75**, 1117 (1997).

102 G. Lu, N. Kioussis, V. V. Bulatov, and E. Kaxiras, Phys. Rev. B **62**, 3099 (2000).

103 W. B. Pearson, *A Handbook of Lattice Spacing and Structure of Metals and Alloys*, vol. 1-2 (Pergamon, Oxford, 1987).

104 P. B. Legrand, Philos. Mag. A **49**, 171 (1984).

105 P. G. Patridge, Met. Rev. **12**, 169 (1967).

106 R. Hultgren, R. L. Orr, P. Anderson, and K. K. Helley, *Selected Values of Thermodynamic Properties of Binary Alloys* (Wiely Internation, New York, 1963).

107 Y. He, R. B. Schwarz, A. Migliori, and S. H. Whang, J. Mater. Res. **10**, 1187 (1995).

108 K. Tanaka and M. Koiwa, Intermetallics **4**, S29 (1996).

109 C. Woodward and J. M. MacLauren, Philos. Mag. A **74**, 337 (1996).

110 J. Ehmann and F. Fahnle, Philos. Mag. A **77**, 701 (1998).

111 P. D. Desai, J. Phys. Chem. Ref. Data **16**, 109 (1987).

¹¹² E. A. Brandes and G. B. Brook, eds., *Smithells Metals Reference Book* (Butterworths, Oxford, 1992).

¹¹³ M. Asta, D. de Fontaine, M. van Schilfgaarde, M. Sluiter, and M. Methfessel, Phys. Rev. B **46**, 5055 (1992).

¹¹⁴ R. Hultgren, P. D. Desai, D. T. Hawkins, M. Gleiser, and K. K. Kelley, *Selected Values of Thermodynamic Properties of Binary Alloys* (American Society for Metals, OH, 1973).

¹¹⁵ K. Tanaka, K. Okamoto, H. Inui, Y. Minonishi, M. Yamaguchi, and M. Koiwa, Philos. Mag. A **73**, 1475 (1996).

Figures

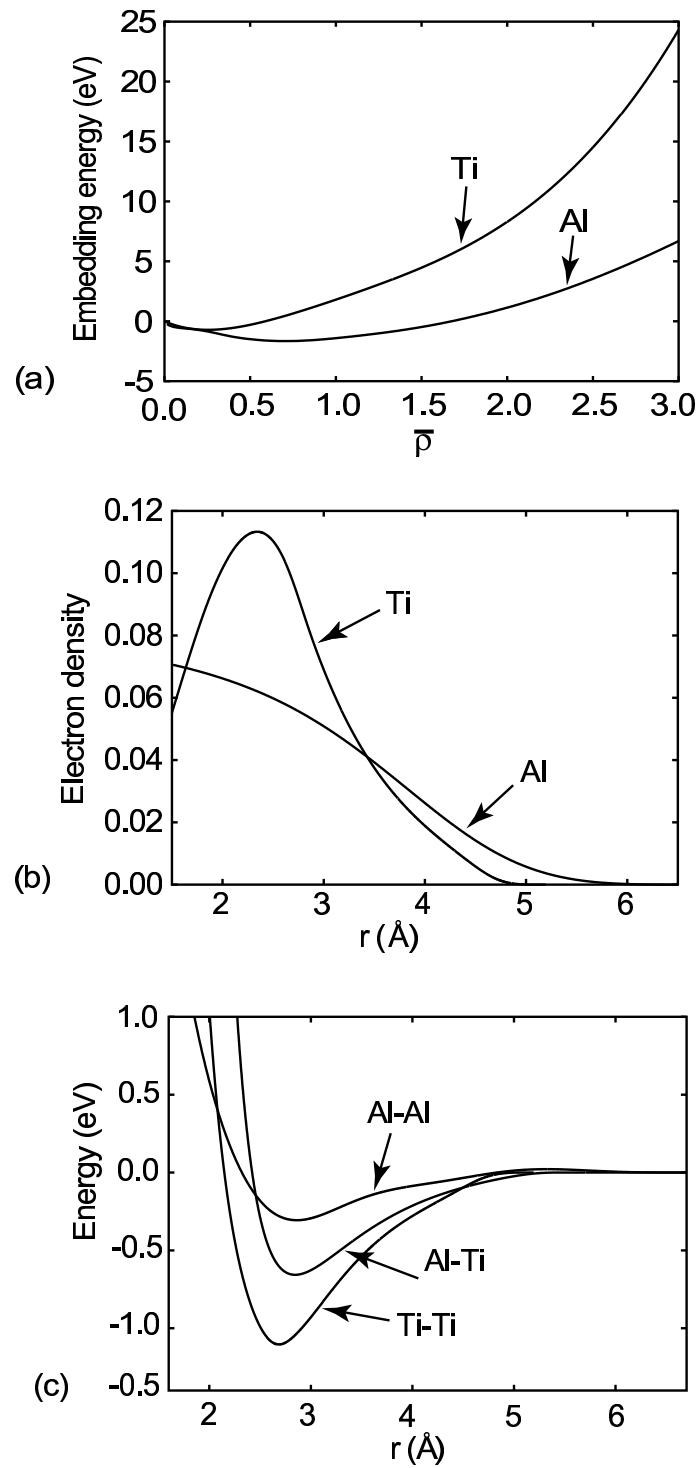


FIG. 1: The embedding energy (a), electron density (in arbitrary units) (b), and the pair interaction function (c) for the Ti-Al system in the effective pair format.

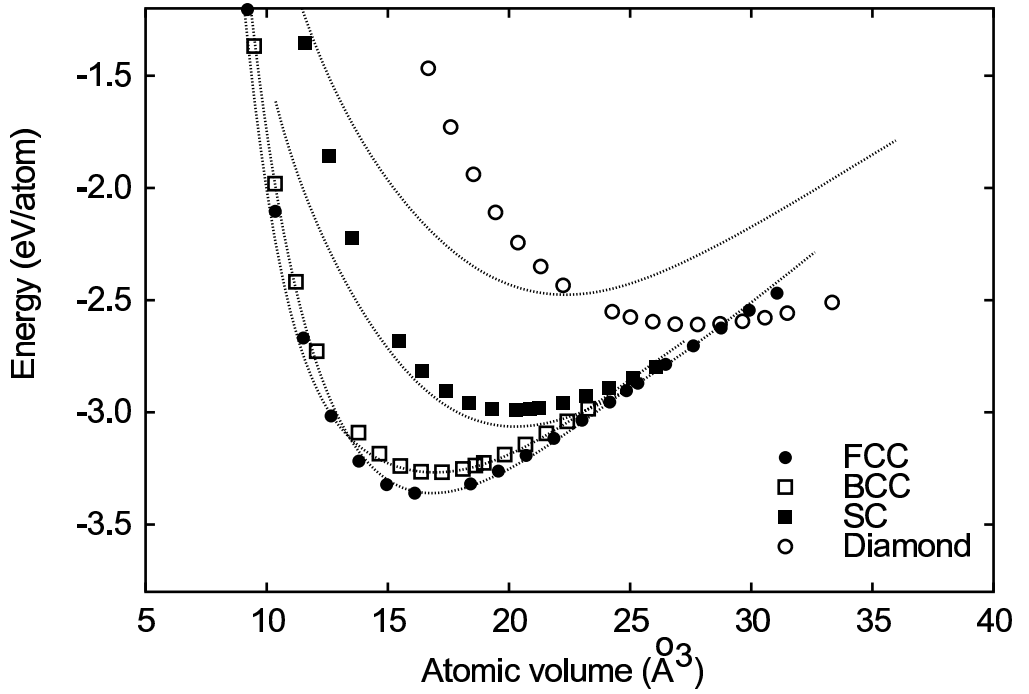


FIG. 2: Energy-volume relations for different crystalline structures of Al calculated with the EAM potential (lines) and by the LAPW method (points).

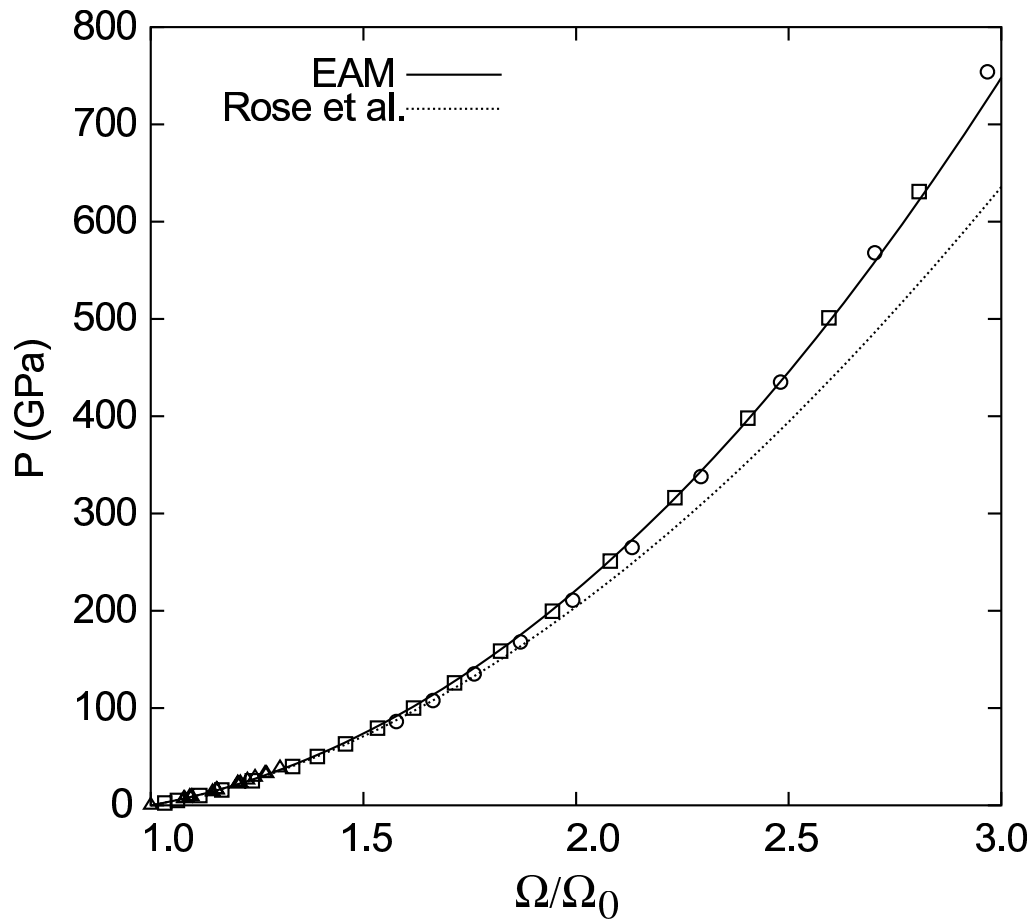


FIG. 3: The pressure-volume relation for aluminum at $T = 0$ calculated with the present EAM potential (solid line), predicted by the universal equation of state⁵⁸ (dotted line), and measured experimentally (squares: Ref. 90; circles: Ref. 91; triangles: Ref. 92).

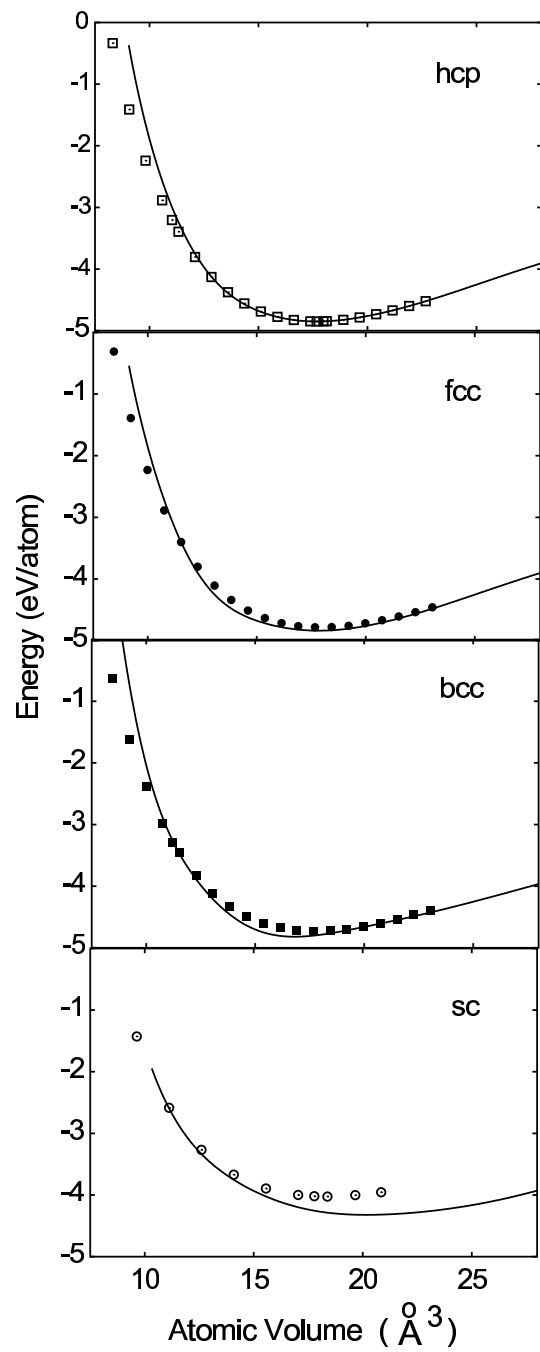


FIG. 4: Comparison of the LAPW (points) and EAM (solid lines) energy-volume relations for different structures of Ti. The LAPW energies were calculated in Ref. 44.

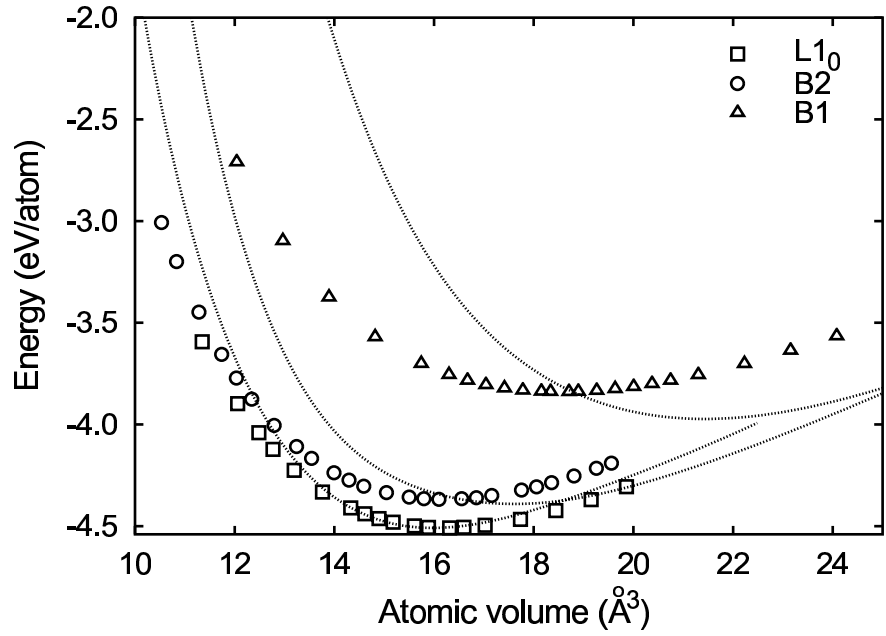


FIG. 5: Energy-volume relations for the $L1_0$, B2 and B1 structures of TiAl. The LAPW results are marked by points, the lines represent EAM calculations.

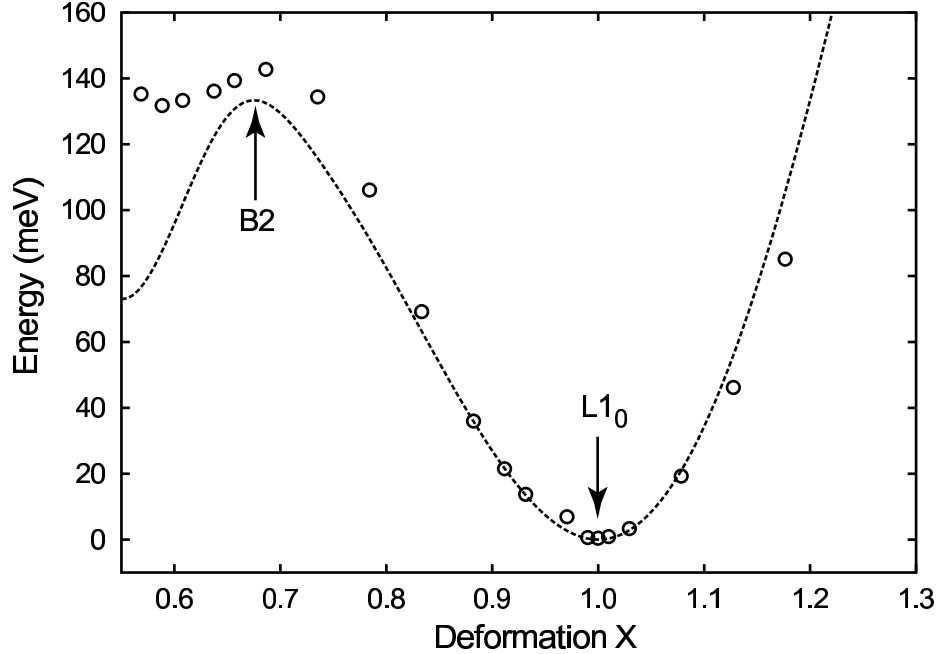


FIG. 6: Energy per atom as a function of the deformation parameter X (see text for details) along the volume conserving tetragonal deformation path (Bain path) in TiAl. The energy is given relative to the equilibrium $L1_0$ structure. The dotted line is predicted by the present EAM potential and the symbols represents the LAPW results.

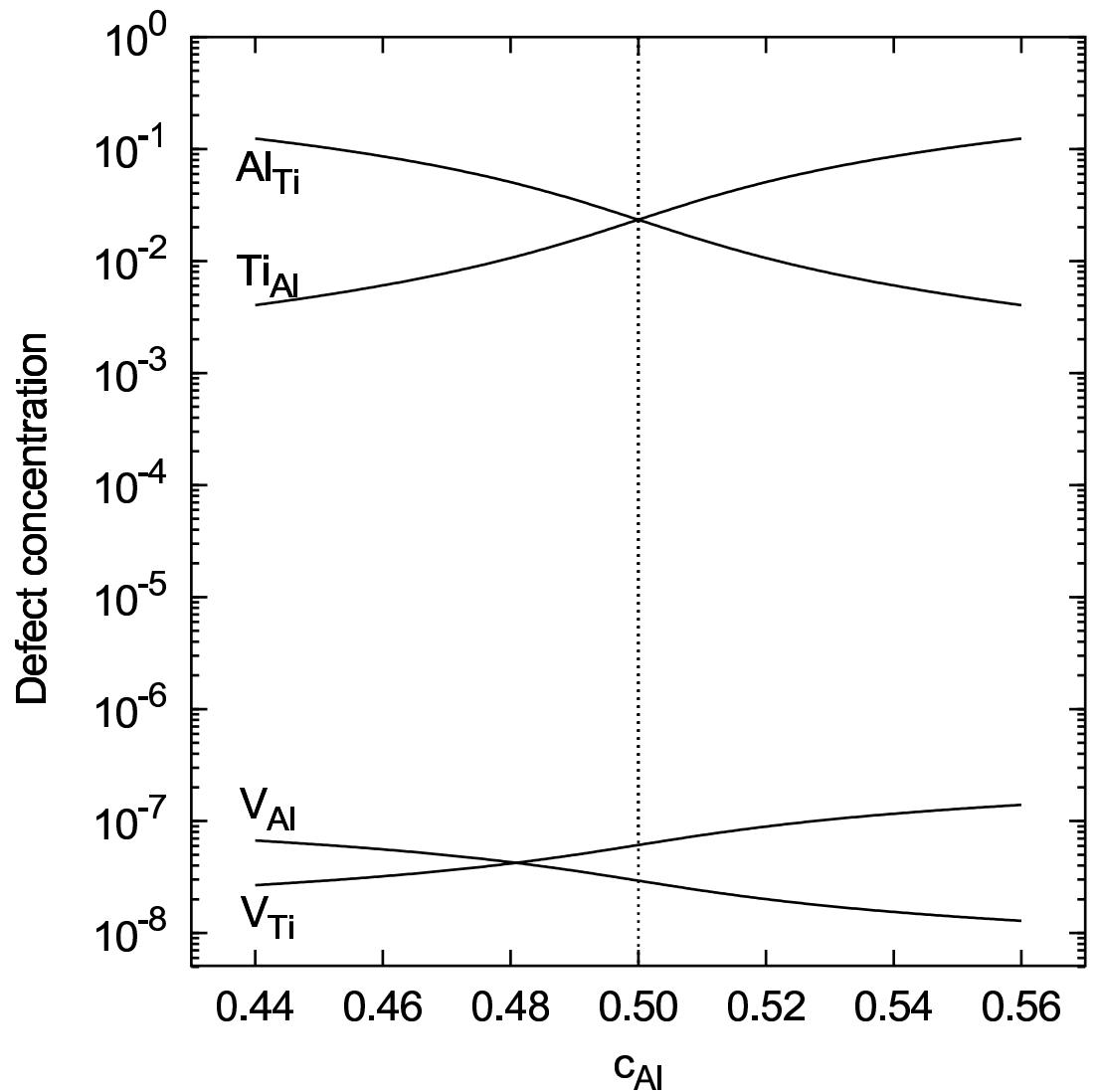


FIG. 7: Calculated equilibrium concentrations of vacancies and antisites in TiAl as functions of the alloy composition at 1000 K.

Tables

TABLE I: Optimized values of the fitting parameters of the EAM potential for the Ti-Al system.

Al		Ti		TiAl	
Parameter	Optimal value	Parameter	Optimal value	Parameter	Optimal value
r_c (Å)	6.724884	r_c (Å)	5.193995	r_c (Å)	5.768489
h (Å)	3.293585	h (Å)	0.675729	h (Å)	0.619767
V_0 (eV)	-3.503182×10^3	V_0 (eV)	-3.401822×10^6	V_0 (eV)	-0.737065
r' (Å)	2.857784	r_1 (Å)	-8.825787	r_0 (Å)	2.845970
b_1	8.595076×10^{-2}	β_1 (1/Å)	5.933482	b_1	5.980610
b_2	5.012407×10^{-2}	V'_0 (eV)	0.161862	b_2	5.902127
δ (eV)	3.750298×10^3	r'_1 (Å)	3.142920	δ (eV)	0.078646
y	2.008047×10^1	β_2 (1/Å)	2.183169	s_{Al}	0.951039
γ (1/Å)	4.279852	δ	-0.601156×10^{-1}	g_{Ti} (eV)	4.839906
B_0 (Å)	1.192727×10^5	A	3.656883×10^2	g_{Al} (eV)	1.281479
C_0 (1/Å ³)	8.60297×10^{-2}	r_0 (Å)	-1.169053×10^1		
r_0 (Å)	0.5275494	r'_0 (Å)	-2.596543×10^2		
β	0.00489	α_1 (1/Å)	0.3969775×10^{-1}		
		α_2 (1/Å)	5.344506×10^2		
		B_1	1.549707		
		B_2	-0.4471131		
		B_3	0.8594003×10^{-1}		

TABLE II: Properties of Al calculated using the present EAM potential and the MFMP potential²⁸ in comparison with experimental data.

Property	Experiment	EAM	MFMP
Lattice properties:			
a_0 (Å)	4.05 ^a	4.05	4.05
E_0 (eV/atom)	3.36 ^b	3.36	3.36
B (GPa)	79 ^c	79	79
C_{11} (GPa)	114 ^c	116.8	113.8
C_{12} (GPa)	61.9 ^c	60.1	61.6
C_{44} (GPa)	31.6 ^c	31.7	31.6
Vacancy:			
E_v^f (eV)	0.68 ^d	0.71	0.68
E_v^m (eV)	0.65 ^e	0.65	0.64
Ω_v^f/Ω_0	0.62 ^f	0.59	0.51
Planar defects:			
γ_{SF} (mJ/m ²)	166 ^g ,120-144 ^h	115	146
γ_{us} (mJ/m ²)		151	168
γ_T (mJ/m ²)	76 ^g	63	76
Surface:			
$\gamma_s(110)$ (mJ/m ²)	980 ⁱ , 1140 ^j , 1160 ^k	792	1006
$\gamma_s(110)$ (mJ/m ²)	980 ⁱ , 1140 ^j , 1160 ^k	607	943
$\gamma_s(111)$ (mJ/m ²)	980 ⁱ , 1140 ^j , 1160 ^k	601	870

^aRef. 93

^bRef. 94

^cRef. 95

^dRef. 96

^eRef. 97

^fRef. 60

^gRef. 98

^hRef. 99 and 100

ⁱAverage orientation, Ref. 98

^jAverage orientation, Ref. 76

^kAverage orientation, Ref. 75

TABLE III: Comparison of the energies (eV/atom) of selected structures of Al calculated by the LAPW method, with the present EAM potential, and with the MFMP potential.²⁸ The energies are given relative to the energy of the equilibrium fcc structure.

Structure	LAPW	EAM	MFMP
hcp	0.04	0.03	0.03
bcc	0.09	0.09	0.011
L1 ₀	0.27	0.33	0.30
sc	0.36	0.30	0.40
diamond	0.75	0.88	0.89

TABLE IV: The linear thermal expansion factor (in %) of Al computed using the present EAM potential in comparison with experimental data at selected temperatures. QHA: quasiharmonic approximation; MC: Monte Carlo method.

T (K)	Experiment ^a	EAM	
		QHA	MC
293	0.418	0.277	0.489
500	0.932	0.663	0.872
700	1.502	1.016	1.332
900	2.182	1.419	1.916

^aRef. 77

TABLE V: Properties of Ti predicted by the present EAM potential and the FMP³⁷ potential in comparison with experimental data.

	Experiment	EAM	FMP ^a
a_0 (Å)	2.951 ^a	2.951	2.951
c/a	1.588 ^a	1.585	1.588
E_0 (eV/atom)	4.850 ^b	4.850	4.850
C_{11} (GPa)	176 ^c	178	189
C_{12} (GPa)	87 ^c	74	74
C_{13} (GPa)	68 ^c	77	68
C_{33} (GPa)	190 ^c	191	188
C_{44} (GPa)	51 ^c	51	50
E_v^f (eV)	1.55 ^d	1.83	1.51
E_v^m (basal) (eV)		0.80	0.51
E_v^m (nonbasal) (eV)		0.83	0.48
Q (eV)	3.14 ^f	2.62	2.02
γ_{I_1} (mJ/m ²)		31	31
γ_{I_2} (mJ/m ²)	290 ^g ,300 ^h	56	57
γ_E (mJ/m ²)		82	84
γ_s (0001) (mJ/m ²)	2100 ⁱ , 1920 ^j	1725	1439

^aRef. 37

^aRef. 103

^bRef. 93

^cRef. 95

^dRef. 63

^fRef. 67

^gRef. 104

^hRef. 105

ⁱAverage orientation, Ref. 75

^jAverage orientation, Ref. 76

TABLE VI: Energies (eV/atom) of selected structures of Ti obtained with the present EAM potential and by the LAPW/GGA-PW91 method.⁴⁴ All energies are given relative to the energy of the experimentally observed hcp structure.

Structure	LAPW/GGA-PW91	EAM	FMP
fcc	0.012	0.011	0.012
bcc	0.067	0.03	0.02
sc	0.77	0.54	0.27
omega	−0.06	0.094	0.064

TABLE VII: The linear thermal expansion factor (in %) of Ti calculated with the present EAM potential in comparison with experimental data at selected temperatures. QHA: quasiharmonic approximation; MC: Monte Carlo method.

T (K)	Experiment ^a	EAM	
		QHA	MC
293	0.15	0.16	0.25
500	0.35	0.38	0.44
700	0.55	0.62	0.63
1000	0.89	1.00	0.72

^aRef. 77

TABLE VIII: Equilibrium lattice constant, c/a ratio, cohesive energy, and elastic constants of γ -TiAl calculated with the present EAM potential in comparison with other potentials^{21,38} and experimental data.

	Experiment	EAM	Ref. 38	Ref. 21
a_0 (Å)	3.997 ^a	3.998	3.951	4.033
c/a_0	1.02 ^a	1.047	1.018	0.991
E_0 (eV/atom)	4.51 ^b	4.509	4.396	4.870
C_{11} (GPa)	186 ^c , 183 ^d	195	222	202
C_{12} (GPa)	72 ^c , 74.1 ^d	107	100	95
C_{13} (GPa)	74 ^c , 74.4 ^d	113	162	124
C_{33} (GPa)	176 ^c , 178 ^d	213	310	237
C_{44} (GPa)	101 ^c , 105 ^d	92	139	83
C_{66} (GPa)	77 ^c , 78.4 ^d	84	76	54

^aRef. 103

^bRef. 106

^cRef. 107

^dRef. 108

TABLE IX: The energies of the superlattice intrinsic stacking fault (SISF), antiphase boundary (APB), complex stacking fault (CSF), and the (100) and (111) surfaces in γ -TiAl calculated with the present EAM potential. Available experimental and *ab-initio* data are included for comparison. All energies are expressed in mJ/m².

	Experiment	<i>ab-initio</i>	EAM
SISF(111)	140 ^a	90 ^b , 110 ^a , 123 ^c , 172 ^d	173
CSF(111)		280 ^a , 294 ^c , 363 ^d	299
APB(111)	250 ^a	510 ^b , 667 ^d , 670 ^a , 672 ^c	266
surface (100)			1177
surface (110)			1445

^aRef. 80

^bRefs. 10,81

^cRef. 109

^dRef. 110

TABLE X: Formation energies, ΔH (eV/atom), of different compounds of the Ti-Al system calculated with the present EAM potential and by the LAPW method in comparison with literature data.

TiAl			Ti ₃ Al		
Structure	ΔH	Method	Structure	ΔH	Method
L1 ₀	-0.404	EAM ^a	DO ₁₉	-0.289	EAM ^a
L1 ₀	-0.43	LAPW/GGA ^a	DO ₁₉	-0.318	LAPW/GGA ^a
L1 ₀	-(0.37-0.39)	Experiment ^b	DO ₁₉	-0.25, -0.26	Experiment ^f
L1 ₀	-0.38	Experiment ^c	DO ₁₉	-0.28	FLASTO/LDA ^d
L1 ₀	-0.41	FLASTO/LDA ^d	DO ₁₉	-0.29, -0.28	LMTO/LDA ^g , FLAPW/LDA ^g
L1 ₀	-0.44	FLMTO/LDA ^e	DO ₁₉	-0.28	FLAPW/LDA ^h
B ₂	-0.27	EAM ^a	L ₁₂	-0.288	EAM ^a
B ₂	-0.29	LAPW/GGA ^a	L ₁₂	-0.30	LAPW/GGA ^a
B ₂	-0.26	FLASTO/LDA ^d	L ₁₂	-0.28	FLASTO/LDA ^d
B ₁	0.13	EAM ^a	L ₁₂	-0.29, -0.27	LMTO/LDA ^g , FLAPW/LDA ^g
B ₁	0.24	LAPW/GGA ^a	DO ₁₁	-0.03	EAM ^a
L1 ₁	-0.30	EAM ^a	DO ₂₂	-0.28	EAM ^a
B32	-0.32	EAM ^a	DO ₂₂	-0.27, -0.25	LMTO/LDA ^g , FLAPW/LDA ^g
“40”	-0.37	EAM ^a	DO ₃	-0.23	EAM ^a

Al ₃ Ti		
Structure	ΔH	Method
DO ₂₂	-0.29	EAM ^a
DO ₂₂	-0.41	FLASTO/LDA ^d
DO ₂₂	-0.42	LMTO/LDA ⁱ
L ₁₂	-0.30	EAM ^a
DO ₃	-0.20	EAM ^a
DO ₁₉	-0.29	EAM ^a

^aPresent work

^bRef. 75,111

^cRef. 112

^dRef. 45

^eRef. 113

^fRefs. 75,114

^gRef. 14

^hRef. 13

ⁱRef. 15

TABLE XI: Equilibrium properties of Ti_3Al predicted by the present EAM potential. *Ab initio* and experimental data are included for comparison.

Property	Experiment	EAM	<i>ab-initio</i>
a_0 (Å)	5.77 ^a	5.784	5.614 ^e
c/a	0.8007 ^a	0.821	0.831 ^e
E_0 (eV/atom)	4.78 ^b	4.766	
C_{11} (GPa)	176.2 ^c , 175 ^d	180.5	221 ^f
C_{12} (GPa)	87.8 ^c , 88.7 ^d	74.4	71 ^f
C_{13} (GPa)	61.2 ^c , 62.3 ^d	70.3	85 ^f
C_{33} (GPa)	218.7 ^c , 220 ^d	222.9	238 ^f
C_{44} (GPa)	62.4 ^c , 62.2 ^d	46.6	69 ^f

^aRef. 103

^bRef. 114

^cRef. 107

^dRef. 115

^eRef. 45

^fRef. 13

TABLE XII: The linear thermal expansion factor (in %) of γ -TiAl calculated with the present EAM potential. QHA: quasiharmonic approximation; MC: Monte Carlo method.

T (K)	EAM	
	QHA	MC
400	0.36	0.53
600	0.66	0.85
800	1.03	1.20
1000	1.54	1.58

TABLE XIII: Energies (in eV) and entropies (normalized to k_B) of point defect complexes in TiAl computed using the present EAM potential. *Ab-initio* results are included for comparison.

Complex	Equation	<i>ab-initio</i> ^a		EAM
		Energy	Energy	Entropy (k_B)
Divacancy	$\epsilon_{V_{Ti}} + \epsilon_{V_{Al}} + 2E_0$	3.582	3.168	2.804
Exchange	$\epsilon_{Al_{Ti}} + \epsilon_{Ti_{Al}}$	1.204	0.765	1.420
Triple-Ti	$2\epsilon_{V_{Ti}} + 2E_0 + \epsilon_{Ti_{Al}}$	3.775	3.525	3.952
Triple-Al	$2\epsilon_{V_{Al}} + 2E_0 + \epsilon_{Al_{Ti}}$	4.593	3.576	3.075
Interbranch Ti	$2\epsilon_{V_{Al}} - \epsilon_{Ti_{Al}} + 2E_0$	3.389	2.810	1.656
Interbranch Al	$\epsilon_{Al_{Ti}} - 2\epsilon_{V_{Ti}} - 2E_0$	-2.571	-2.759	-2.532

^aRef. 86